A Study To Control Chemical Reactions Using Si:2p Core Ionization: Site-Specific Fragmentation

ARTICLE *in* THE JOURNAL OF PHYSICAL CHEMISTRY A · AUGUST 2011

Impact Factor: 2.69 · DOI: 10.1021/jp203664r · Source: PubMed

THE JOURNAL OF PHYSICAL CHEMISTRY A

ARTICLE

pubs.acs.org/JPCA

A Study To Control Chemical Reactions Using Si:2p Core Ionization: Site-Specific Fragmentation

Shin-ichi Nagaoka,*[,†] Hironobu Fukuzawa,[‡] Georg Prümper,[‡] Mai Takemoto,[†] Osamu Takahashi,[§] Katsuhiro Yamaguchi,[†] Takuhiro Kakiuchi,[†] Kiyohiko Tabayashi,[§,#] Isao H. Suzuki,[∥] James R. Harries,[⊥,&] Yusuke Tamenori,[⊥] and Kiyoshi Ueda[‡]

[†]Department of Chemistry, Faculty of Science and Graduate School of Science and Engineering, Ehime University, Matsuyama 790-8577, Japan

[‡]Institute of Multidisciplinary Research for Advanced Materials, Tohoku University, Sendai 980-8577, Japan

[§]Department of Chemistry, Graduate School of Science, Hiroshima University, Higashi-Hiroshima 739-8526, Japan

[∥]Institute of Materials Structure Science, High Energy Accelerator Research Organization (KEK), 1-1 Oho, Tsukuba 305-0801, Japan

[⊥]Japan Synchrotron Radiation Research Institute/SPring-8, 1-1-1 Kouto, Sayo-cho, Sayo-gun 679-5198, Japan

Supporting Information

ABSTRACT: In an aim to create a "sharp" molecular knife, we have studied site-specific fragmentation caused by Si:2p core photoionization of bridged trihalosilyltrimethylsilyl molecules in the vapor phase. Highly site-specific bond dissociation has been found to occur around the core-ionized Si site in some of the molecules studied. The site specificity in fragmentation and the 2p binding energy difference between the two Si sites depend in similar ways on the intersite bridge and the electronegativities of the included halogen atoms. The present experimental and computational results show that for efficient "cutting" the following conditions for the two atomic sites to be separated by the knife should be satisfied. First, the sites should be located far from each other and connected by a chain of saturated bonds so that intersite electron migration can be reduced. Second, the chemical environments of the atomic sites should be as different as possible.

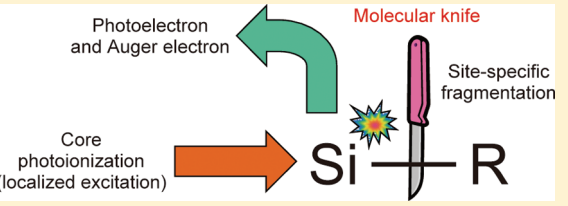

1. INTRODUCTION

A pair of scissors is convenient for cutting a corner from a sheet of paper, and for a very small piece of paper we would usually use a knife. However, there is yet no appropriate tool for "cutting" a nanoscale device, a molecular assembly, or a molecule. Such a tool would be useful for controlling chemical reactions and also offers possibilities for analyzing the structures and properties of the above-mentioned small objects by controlling matter at the level of individual atoms. As a candidate for such a "molecular knife", one may consider localized photoexcitation. In contrast to valence electrons, which are delocalized over the entire molecule, core (inner-shell) electrons are localized very close to the nucleus of one particular atom. Thus, controlled bond dissociation following photoexcitation or photoionization of a localized core electron can be expected to work as a molecular knife.[1,2] In this scenario, we would first select a particular atom and then target it with the "molecular knife" of core photoexcitation or photoionization, with the aim of causing localized bond dissociation at the target site.

To distinguish between atoms of different elements within a molecule, we can make use of core-electron binding energy differences.[3] For example, Hitchcock and Neville could selectively photoexcite a P:2p core electron in SPF_3 since the difference in binding energies between the S:2p and P:2p core electrons is very large (about 35 eV).[4] As a result, they could study selectively the fragmentation processes caused by photoexcitation at each site. Although this was described as "site-selective" fragmentation, a more accurate term would be "element-specific" fragmentation since the excited 2p electrons belonged to two different elements:[5] sulfur and phosphorus. Element-specific fragmentation is potentially useful for controlling chemical reactions and also offers possibilities as a molecular knife.

True site specificity is much more difficult, since it requires the selection between atoms of the same element but with differing chemical environment—for example, the two carbon atoms in CF_3CH_3.[6,7] To achieve this, we can use the shift in core-electron binding energy which occurs due to the specific chemical environment—the "chemical shift" essential for ESCA (electron spectroscopy for chemical analysis).[8,9] The ESCA chemical shift energy differences (for example, about 6.5 eV between the two carbon atoms of CF_3CH_3)[6] are generally much smaller than the core-electron binding energy differences among different elements. By using the ESCA chemical shift, a specific

Received: April 19, 2011
Revised: July 13, 2011
Published: July 13, 2011

Chart 1. Structures of the HSMSB Molecules Studied in the Present Work

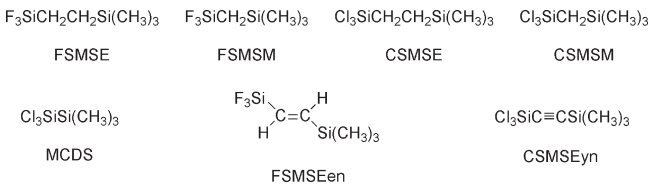

fragmentation process caused by a core-electron photoexcitation at one atom inside a molecule can be distinguished from a process at another atom of the same element in a different chemical environment. In this paper, we term this "site-specific fragmentation". Site-specific fragmentation can provide a more precise molecular knife than element-specific fragmentation. To realize this exciting tool, we need to understand what controls fragmentation at the level of an atom in a particular chemical environment.

Site-specific fragmentation was first reported for C:1s photoexcitations in acetone (CH_3COCH_3) vapor by Eberhardt et al.,[10] but the site specificity was not confirmed by Suzuki and Saito.[11,12] When the atomic sites are interconnected to each other as in acetone, intersite electron migration may efficiently take place, and the site-specific fragmentation may not clearly be revealed. Accordingly, the choice of target molecule is important. Especially, the role of the bridge between the atomic sites on the site specificity should carefully be investigated by means of modern sophisticated spectroscopy and advanced computational methods, since the bridge length and the bond order within the bridge may have a great influence on the site specificity.

Site-specific fragmentation on surfaces or in bulk material is also very interesting,[13−15] and its study has some advantages compared with that in the vapor phase. However, on surfaces or in bulk material, reneutralization and recapture by the substrate or nearby molecules can blur the fragmentation pattern intrinsic to the isolated molecule, and fast energetic processes may dominate.[16] As a result, comparison between experimental results and computational results for the isolated molecule can become difficult. Accordingly, the above-mentioned investigation on the site-specific fragmentation is best performed in the vapor phase.

In this work we have experimentally and computationally studied site-specific fragmentation caused by Si:2p core photoionization in bridged trihalosilyltrimethylsilyl molecules $X_3SiC_nH_mSi(CH_3)_3$, where n = 0−2, m = 0−4, and X = F or Cl—abbreviated hereafter as HSMSB (halosilylmethylsilyl bridge) molecule. The experiments were performed in the vapor phase. Site-specific fragmentation of Si-containing molecules such as HSMSBs draws the attention of a lot of researchers, since Si materials are often used for fabrication of electronic devices; this fabrication has become very precise in recent years,[17,18] and there is a real need for a "molecular knife" in this area. Furthermore, HSMSB molecules are useful for the study of site-specific fragmentation because the chemical environment of the Si atom bonded to three halogen atoms (here denoted Si[X]) is very different from that of the Si atom bonded to three methyl groups (Si[Me]). Whereas halogen atoms are electron acceptors with a large electronegativity, methyl groups are electron donors with a small electronegativity.[19] A previous rapid communication[20] showed clear evidence for almost 100% site specificity in Si:2p photoionization of one particular HSMSB molecule in the vapor phase: 1-trifluorosilyl-2-trimethylethane ($F_3SiCH_2CH_2Si(CH_3)_3$, FSMSE, Chart 1). Fragmentation induced by Si:1s ionization is more destructive than that caused by the Si:2p ionization.[5] However, the reasons for the high site specificity of FSMSE, the dependence of the site specificity on the characteristics of the bridge between the two Si sites (length and bond order) in HSMSBs, and the site specificity difference between F- and Cl-substituted HSMSBs have not yet been elucidated. Accordingly, to create a "sharper" molecular knife, we have investigated the site-specific fragmentation of HSMSBs using an electron−ion coincidence technique and ab initio molecular orbital (MO) calculations.

2. EXPERIMENTAL SECTION

2.1. Sample Preparation. Chart 1 shows the structures of the HSMSB molecules used in the present work. The preparation of FSMSE, (trifluorosilyl)(trimethylsilyl)methane [$F_3SiCH_2Si(CH_3)_3$, FSMSM], 1-trichlorosilyl-2-trimethylsilylethane [$Cl_3SiCH_2CH_2Si(CH_3)_3$, CSMSE], (trichlorosilyl)(trimethylsilyl)methane [$Cl_3SiCH_2Si(CH_3)_3$, CSMSM], 1,1,1-trimethyltrichlorodisilane [$Cl_3SiSi(CH_3)_3$, MCDS], (*E*)-1-trifluorosilyl-2-trimethylsilylethene [$F_3SiCH{=}CHSi(CH_3)_3$, FSMSEen], and 1-trichlorosilyl-2-trimethylsilylethyne [$Cl_3SiC{\equiv}CSi(CH_3)_3$, CSMSEyn] has been reported in previous papers.[21−24] Because a methyl group and a F atom tend to become exchanged in 1,1,1-trimethyltrifluorodisilane [$F_3SiSi(CH_3)_3$], we could not prepare it. It was also not possible to organically synthesize 1-trifluorosilyl-2-trimethylsilylethyne [$F_3SiC{\equiv}CSi(CH_3)_3$].

2.2. Measurements. Electron−ion coincidence measurements for HSMSB vapor were performed by using a hemispherical electron energy analyzer (Gammadata-Scienta SES-2002) and a time-of-flight (TOF) ion spectrometer, each of which was equipped with a position-sensitive delay-line detector.[25,26] The coincidence apparatus was mounted behind the high-resolution plane-grating monochromator installed on the c branch of the soft X-ray figure-8 undulator beamline 27SU at the SPring-8 facility.[27] The setup and experimental procedure have been described in a previous paper[20] and its electronic physics auxiliary publication service (EPAPS) document. By recording a photoelectron spectrum (PES) of mixed gas of each HSMSB and Kr, the Si:2p binding energy of the HSMSB was calibrated with respect to the binding energy of Kr:$3d_{5/2}$ (93.83 eV).[28]

3. COMPUTATIONAL METHOD AND PROCEDURE

The Gaussian 03 program[29] was used for the geometry optimization of each HSMSB, without any symmetry constraints, at the MP2/cc-pVDZ level. The basic computational method and procedure used in the ab initio MO calculation of the Auger electron spectrum (AES) and the bond dissociation factor (BDF) of HSMSB were described in detail in a previous paper.[30] The BDF gives a measure of the ease/difficulty in dissociating a particular bond after core photoionization and the subsequent Auger decay.

To understand the experimental results more thoroughly, we have made some modifications to the computational scheme in the present study. To estimate the Auger final state, a configuration interaction (CI) calculation within the valence-two-hole space was performed. Löwdin's population scheme was applied to the evaluation of the atomic populations of valence MOs on a

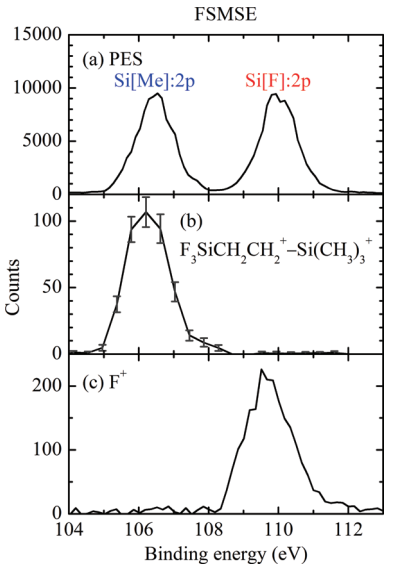

Figure 1. (a) Si:2p PES of FSMSE vapor.[20] (b) PEPIPICO counts for the $F_3SiCH_2CH_2^+-Si(CH_3)_3^+$ fragment ion pair.[20] (c) PEPICO counts for F^+.[5] The spectra shown in the figure and all the PES given in this paper are plotted as a function of the photoelectron binding energy.

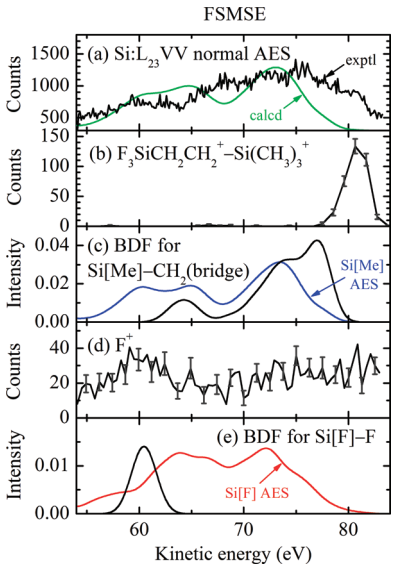

Figure 2. (a) Experimentally observed Si:L_{23}VV normal AES of FSMSE vapor (black line)[20] and the computational spectrum (green line), which is the sum of the two spectra shown in panels c and e. The vertical scale is for the experimental AES, and the computational AES has been scaled to facilitate comparison. (b) AEPIPICO counts for the $F_3SiCH_2CH_2^+-Si(CH_3)_3^+$ ion pair.[20] (c) Plot of the BDF computed for Si[Me]–CH_2(bridge) by Si[Me]:2p ionization (black line) and computational Si:L_{23}VV normal AES after creation of a Si[Me]:2p core hole (blue line). (d) AEPICO counts for F^+.[20] (e) Plot of the BDF computed for Si[F]–F by Si[F]:2p ionization (black line) and the computational Si:L_{23}VV normal AES after creation of a Si[F]:2p core hole (red line). The spectra shown in Figure 2 are plotted as a function of the Auger-electron kinetic energy. In panels c and e, the vertical scale is for the BDF plot, and the computational AES has been scaled to facilitate comparison.

Si:2p core-ionized atom. The Auger transition probability (the AES) was estimated with the atomic populations. The differences in Auger transition probability between population schemes were discussed in a previous paper.[31] Although the initial state of the Auger decay is the Si:2p core-hole state, the present calculations were performed by using the ground-state MOs because they could reproduce the experimentally observed spectra better than those using the core-hole MOs. In evaluation of the BDF, the bond order for the chemical bond was estimated with Mulliken's population scheme. The cc-pCVTZ basis set was employed in the evaluation of the Auger transition probability and the BDF. Probabilities of normal Auger-electron transitions from a doublet core-ionized state to triplet doubly ionized states seem to be much less than those of the corresponding singlet transitions.[32] To reach a triplet doubly ionized state in a closed-shell molecule, the two electrons involved in the Auger decay must have parallel spin. If the spatial orbitals for these electrons are the same, the resulting probability for the triplet transition is zero. Singlet transitions are strongly favored especially for transitions producing high kinetic energy Auger electrons.[33] Accordingly, we took only the singlet transitions into account in the evaluation of the BDF unless otherwise noted. Because of the above-mentioned modifications to the computational scheme, the calculated spectra are slightly different from those in ref 34.

In the plots of the computed AES and BDF as functions of Auger-electron kinetic energy, Gaussian convolution was performed with a width of 2.5 eV. In the BDF plot, we neglected values less than 0.003.

4. RESULTS AND DISCUSSION

4.1. General Remarks. In a HSMSB molecule the two Si atoms—Si[X] and Si[Me]—have different chemical environments, leading to two energy-resolved Si:2p-photoelectron peaks reflecting the different ESCA chemical shifts (for example, see Figure 1a). The reason for this chemical shift difference has been explained in detail previously.[8,19,22] Little molecular deformation is induced by the Si:2p core-hole formation because the curvature of the potential energy surface of the core-ionized state is small in the Franck–Condon region, and the atoms then involved in the deformation are heavy.[20]

Following Si[X]:2p photoelectron emission in a HSMSB molecule, a valence electron fills the Si[X]:2p hole, creating a valence hole that spatially overlaps the Si[X] site ($HSMSB^+$). The electron falling into the Si[X]:2p hole usually gives its energy to another valence electron, which is emitted as a Si[X]:L_{23}VV normal Auger electron, creating a second valence hole ($HSMSB^{2+}$). Since these valence holes weaken the chemical bonds around the initially core-ionized Si[X] atom, site-specific fragmentation ($HSMSB^{2+} \rightarrow F_1^+ + F_2^+$, where F_1 and F_2 denote fragments) often occurs around the Si[X] site. To observe such a fragmentation process selectively, we have to selectively detect the ion pairs ($F_1^+-F_2^+$) produced through the Si[X]:2p photoelectron emission. For this purpose, energy-selected photoelectron–photoion–photoion triple-coincidence (PEPIPICO) spectroscopy is an effective technique.[20] The same situation is valid for Si[Me]:2p photoelectron emission. The Si atoms of SiX_4 and $Si(CH_3)_4$ can respectively be regarded as models of the Si[X] and Si[Me] sites in HSMSB having an intersite bridge of infinite length ($n = \infty$). As expected, bond dissociation caused by Si:2p photoionization in $Si(CH_3)_4$ occurs around the Si atoms[21] as well as that in SiX_4.[35−37]

In contrast to the Si:2p photoelectron spectrum (PES) of HSMSB, the Si:L_{23}VV normal Auger-electron spectrum (AES) is not clearly resolved site by site (for example, see Figure 2a); only

dx.doi.org/10.1021/jp203664r |J. Phys. Chem. A 2011, 115, 8822–8831

shoulders can be seen in the spectrum.[34] Those normal Auger transitions lead to various doubly ionized states (Auger final states). To elucidate the site-specific fragmentation process in detail, we have to deduce the characters of these Auger final states by using the ab initio MO method. From the calculations AES spectral features such as the above-mentioned shoulders may be assigned to the Auger final states. Furthermore, we have to selectively detect the ion pairs ($F_1^+-F_2^+$) produced through these states by means of energy-selected Auger-electron−photoion−photoion triple-coincidence (AEPIPICO) spectroscopy.

Since PEPIPICO spectroscopy correlates energy-resolved photoelectron emission with ion-pair production, we can selectively detect an ion pair produced through core photoelectron emission from one Si site, in distinction from that from the other Si site. The AEPIPICO spectroscopy similarly correlates Auger-electron emission with its resultant ion-pair production. AEPIPICO can potentially offer selective detection of an ion pair produced through an Auger final state though actually such selective detection is often very difficult in large molecules. It should be noted that a mixture of the process initiated by the Si[X]:2p emission and the process initiated by the Si[Me]:2p emission is observed in AEPIPICO for Si:L_{23}VV of HSMSB because the initially core-ionized Si site is not specified and the AES is not clearly resolved site by site. Similarly, in the Si[X]:2p PEPIPICO, a mixture of the processes through various Si[X]:L_{23}VV normal Auger final states is observed because the Auger initial-state (Si[X]:2p core-ionized state) is specified, but its Auger final state is not specified. The same supposition is valid for the Si[Me]:2p PEPIPICO. In this paper we report site-specific fragmentation in HSMSB vapor studied using PEPIPICO and AEPIPICO spectroscopy.

On the other hand, correlation between core photoelectron emission and Auger-electron emission is interesting for studying electronic transitions induced by the core ionization. This can potentially be studied using Auger photoelectron coincidence spectroscopy (APECS). However, it is not within the scope of this paper to present APECS for HSMSB, and the results of APECS for condensed FSMSE will be reported elsewhere.[15]

4.2. FSMSE. In a previous rapid communication,[20] we reported site-specific fragmentation caused by Si:2p photoionization in FSMSE vapor. To help understand some of the points raised in the present paper, our previous experimental results are summarized below together with the present computational results.

Figure 1a shows the Si:2p PES of FSMSE vapor. The spectra shown in Figure 1 and all the PES given in this paper are plotted as a function of the photoelectron binding energy. The PES of FSMSE has two peaks, and the peaks at lower and higher binding energies are respectively assigned to the Si[Me]:2p and Si[F]:2p core-ionized states, whose energies[38] and the difference between them are given in Table S1 (Supporting Information) together with those of the other HSMSB.

Figure 1b shows a plot of the $F_3SiCH_2CH_2^+-Si(CH_3)_3^+$ ion pair PEPIPICO counts from FSMSE against the photoelectron binding energy. A peak is seen at the Si[Me]:2p binding energy, whereas the PEPIPICO count rate is negligible at the Si[F]:2p binding energy. Thus, the Si[Me] site specificity for $F_3SiCH_2CH_2^+-Si(CH_3)_3^+$ production following Si:2p photoionization in FSMSE is almost 100%, showing that the Si[Me]−CH_2(bridge) bond dissociation is site specifically induced by Si[Me]:2p ionization. The bond dissociation factor (BDF) computed for the Si[Me]−CH_2(bridge) following Si[Me]:2p ionization (0.31) is much greater than that calculated for Si[F]:2p ionization (0.08) in FSMSE, consistent with the experimental results.

Ionic fragmentation induced by Si:2p photoionization in FSMSE produces various F^+-containing ion-pairs (F^+-R^+, where R^+ denotes the counterpart ion to F^+). The sum of the F^+-R^+ PEPIPICO spectra over all possible R^+ corresponds to the photoelectron photoion coincidence (PEPICO) spectrum for F^+. This is shown in Figure 1c. A peak is seen at the Si[F]:2p binding energy, whereas the PEPICO count is negligible at the Si[Me]:2p binding energy. Thus, the Si[F] site specificity for F^+ production following Si:2p photoionization in FSMSE is also almost 100%, showing that Si[F]−F bond dissociation to form F^+ is site specifically induced by Si[F]:2p ionization. The BDF computed for Si[F]−F by Si[F]:2p ionization (0.12 per bond) is much greater than that computed for Si[Me]:2p ionization (0.05 per bond) in FSMSE, supporting the experimental results.

In addition to the above-mentioned fragmentation, the complete range of site-specific fragmentation patterns caused by Si:2p ionization in FSMSE vapor was summarized in Figure 6 of ref 5 and its EPAPS document. Highly site-specific bond dissociation occurs around the Si site where the photoionization has taken place. The BDF values of FSMSE are given in Table S2 (Supporting Information).

Figure 2a shows the experimental and computational Si:L_{23}VV normal Auger-electron spectra for FSMSE. In contrast to the photoelectron spectrum (Figure 1a), site-specific peaks are not resolved. The peaks and shoulders of the computational spectrum are at slightly lower kinetic energies than the corresponding peaks in the experimental spectrum. This may be at least partly due to the CI calculation being limited to the two valence-hole space.

Figure 2b shows the AEPIPICO counts for $F_3SiCH_2CH_2^+-Si(CH_3)_3^+$, a site-specific ion pair formed by Si[Me]:2p photoionization in FSMSE (see Figure 1b). A single peak is seen at the same position as the high kinetic energy shoulder of the experimentally observed Auger band (Figure 2a). This indicates that Si[Me]−CH_2(bridge) bond dissociation to form $F_3SiCH_2CH_2^+-Si(CH_3)_3^+$ is a result of the highest kinetic energy Auger decay. Figure 2c shows the plot of the computed BDF for Si[Me]−CH_2(bridge) for Si[Me]:2p ionization (black line) and also the calculated Si:L_{23}VV normal AES after creation of a Si[Me]:2p core hole (blue line) in FSMSE. The BDF plot also has a peak at the same position as the shoulder at the high kinetic energy edge of the computational Si[Me]:L_{23}VV normal Auger band. As in the normal Auger spectra (Figure 2a), the peak in the calculated BDF (Figure 2c) is at a lower kinetic energy than the peak seen in the experimental AEPIPICO plot (Figure 2b). However, the computational result that Si[Me]−CH_2(bridge) bond dissociation by Si[Me]:2p ionization is enhanced at the highest kinetic energy edge (Figure 2c) is consistent with the experimental result (Figure 2b and black line in Figure 2a). The Auger final state at the highest kinetic energy edge has two holes in valence MOs which have Si[Me]−CH_2(bridge) bonding character ($\sigma_{Si[Me]-CH_2(bridge)}$) with high probability.[20] Hole creation in $\sigma_{Si[Me]-CH_2(bridge)}$ is thought to result in the Si[Me]−CH_2(bridge) bond dissociation and the $F_3SiCH_2CH_2^+-Si(CH_3)_3^+$ production.

The BDF in Figure 2c has a nonnegligible value in a wide region (60−80 eV), while the experiment has a definitely higher selectivity reporting a signal in a definitely narrower region near 80 eV (Figure 2b). The reason for this is that the experimental signal given in Figure 2b shows only the

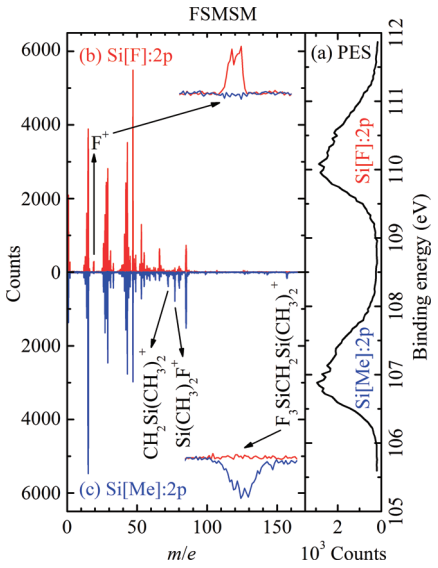

Figure 3. (a) Si:2p PES of FSMSM vapor. (b) and (c) Mass spectra (PEPICO spectra) of ions produced through Si[F]:2p and Si[Me]:2p core-ionized states, respectively. The insets show the regions corresponding to F^+ and $F_3SiCH_2Si(CH_3)_2^+$ on enlarged scales.

$F_3SiCH_2CH_2^+-Si(CH_3)_3^+$ production from $FSMSE^{2+}$, whereas the BDF curve in Figure 2c reflects all the processes following the Si[Me]−CH_2(bridge) bond dissociation in $FSMSE^{2+}$, a part of which is the $F_3SiCH_2CH_2^+-Si(CH_3)_3^+$ production. As mentioned above, the Si[Me]−CH_2(bridge) bond dissociation and the $F_3SiCH_2CH_2^+-Si(CH_3)_3^+$ production occur at the highest kinetic energy edge of the Auger band. However, as the Auger-electron kinetic energy decreases, the resultant Auger final state has higher energy and its two holes occupy deeper valence MOs.[7] As a result, some disintegration leading to smaller species occurs with the Si[Me]−CH_2(bridge) bond dissociation in $FSMSE^{2+}$.

The sum of the F^+-R^+ AEPIPICO counts over all possible R^+ corresponds to the Auger-electron−photoion coincidence (AEPICO) counts for F^+. Figure 2d shows the AEPICO spectrum for F^+, a site-specific ion formed by Si[F]:2p photoionization in FSMSE (Figure 1c). A broad peak is seen at about 60 eV, and a similar result has also been reported in a condensed phase study.[15] Furthermore, the plot of the BDF computed for Si[F]−F after Si[F]:2p ionization also has a peak at about 60 eV for FSMSE (black line in Figure 2e), and the Auger final state at about 60 eV has two valence MO holes with Si[F]−F bonding character ($\sigma_{Si[F]-F}$) with high probability.[20] All of the above-mentioned experimental and computational results suggest that Si[F]−F bond dissociation forming F^+ is a result of an Auger decay at about 60 eV. However, the signal-to-background ratio for the peak at 60 eV in Figure 2d is small in comparison to the clear peak for $F_3SiCH_2CH_2^+-Si(CH_3)_3^+$ in Figure 2b. Furthermore, in the computational Si:L_{23}VV normal AES after creation of a Si[F]:2p core hole (red line in Figure 2e), the transition corresponding to the BDF peak at about 60 eV is too small to be seen. Accordingly, the formation of F^+ may also take place through a variety of Si[F]:L_{23}VV normal Auger final states in addition to that at about 60 eV.

4.3. FSMSM. Figure 3a shows the Si:2p PES of FSMSM, in which the bridge between the Si[F] and Si[Me] sites is $-CH_2-$, one methylene unit shorter than that of FSMSE ($-CH_2CH_2-$). As in FSMSE, the Si:2p PES of FSMSM has two peaks, and the

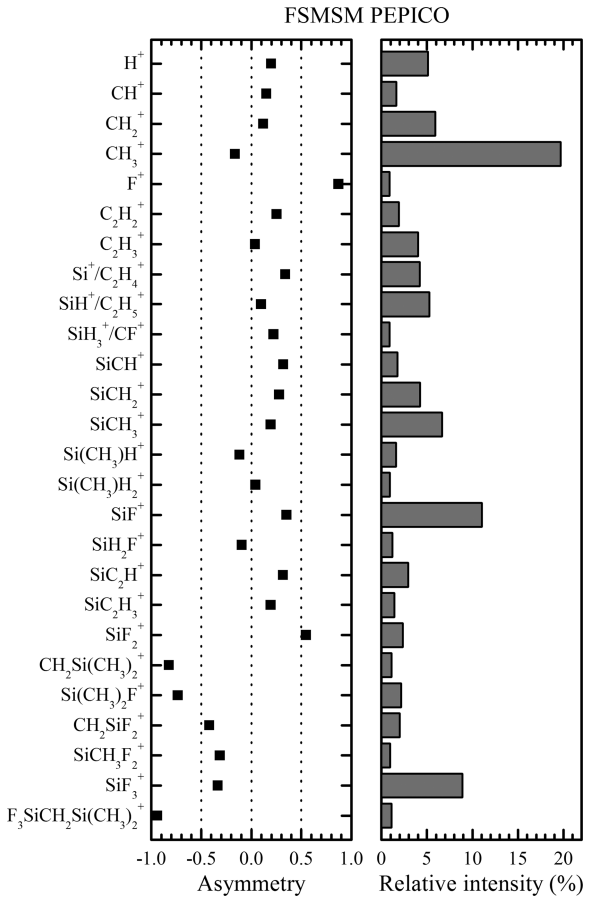

Figure 4. Asymmetry and relative intensity in ion formation following Si:2p photoionization in FSMSM vapor.

peaks at lower and higher binding energies are respectively assigned to the Si[Me]:2p and Si[F]:2p core-ionized states. The binding energy difference (chemical shift) between Si[F]:2p and Si[Me]:2p in FSMSM (3.2 eV) is less than that in FSMSE (3.4 eV), as shown in Table S1.

The mass spectra of the ions produced through the Si[F]:2p and Si[Me]:2p core-ionized states (PEPICO spectra) in FSMSM are shown in Figures 3b and 3c, respectively. Site-specific fragmentation is clearly revealed. The fragment ions most sensitive to the site of the initial energy deposition are F^+ and $F_3SiCH_2Si(CH_3)_2^+$, whose production is enhanced by Si[F]:2p and Si[Me]:2p photoionizations, respectively. The site specificity for the production of these ions is almost 100%.

Here we introduce an asymmetry parameter for evaluation of the site specificity in fragmentation. This is the same parameter which was described in previous papers (ref 39 and EPAPS documents of refs 5 and 20).

$$\begin{aligned} asymmetry &= (a-b)/(a+b) \\ a &= A/AN \\ b &= B/BN \end{aligned} \quad (1)$$

Here A and B denote the numbers of mass-selected ions produced through the Si[F]:2p and Si[Me]:2p core-ionized states, respectively. AN and BN stand for the numbers of the Si[F]:2p and Si[Me]:2p photoelectrons, respectively. This definition of the asymmetry ensures that if the Si[F]:2p and

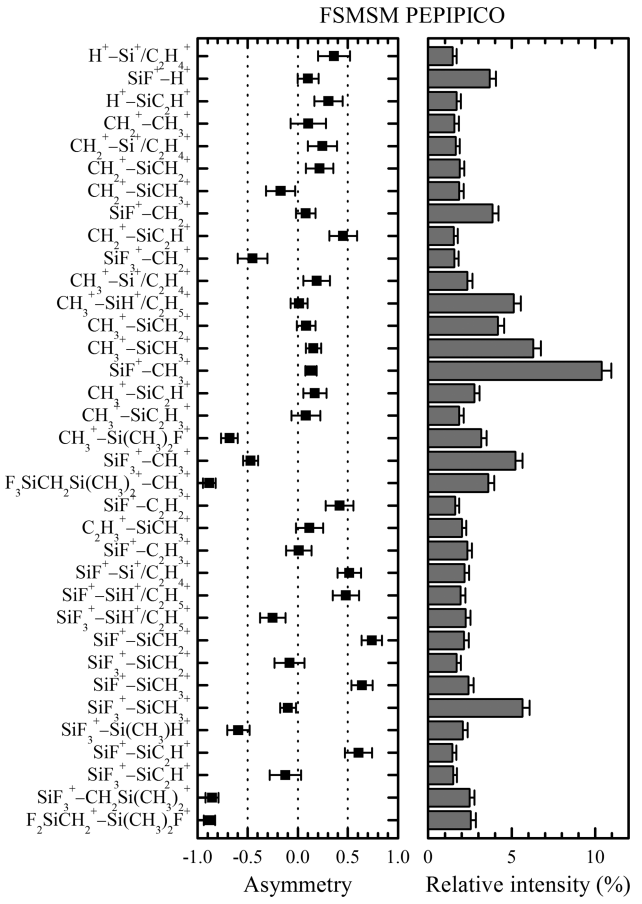

Figure 5. Asymmetry and relative intensity in ion-pair formation following Si:2p ionization in FSMSM vapor.

Si[Me]:2p photoionizations lead to the same fragmentation pattern, the asymmetry of every ionic fragment is zero. If ions of a specific mass are produced only through the Si[F]:2p photoelectron emission, the asymmetry is +1, and if ions of another specific mass are produced only through the Si[Me]:2p photoelectron emission, the asymmetry is −1.

Figure 4 shows the asymmetry and relative intensity of each ion produced by Si:2p photoionization in FSMSM. The relative intensity refers to the branching ratio of the total ion count into each ion. Si[Me]:2p ionization preferentially leads to the production of $CH_2Si(CH_3)_2^+$, $Si(CH_3)_2F^+$, and $F_3SiCH_2Si(CH_3)_2^+$, and Si[F]:2p photoionization leads to the production of F^+ and SiF_2^+.

Figure 5 shows the asymmetry and relative intensity for the formation of ion pairs following Si:2p ionization in FSMSM. For these PEPIPICO results the asymmetry (eq 1) was calculated with *A* and *B* denoting the numbers of ion pairs produced through the Si[F]:2p and Si[Me]:2p core-ionized states, respectively. Whereas Figures 3b and 4 show that the fragment ions showing the most Si[F] site specificity are F^+ and SiF_2^+, the PEPIPICO counts for pairs containing these fragments are very low and not shown in Figure 5. However, Figure 5 shows that Si[F]:2p ionization (positive asymmetry parameter) increases the production of SiF^+-containing ion pairs ($SiF^+-SiCH_2^+$, $SiF^+-SiCH_3^+$, and $SiF^+-SiC_2H^+$). The SiC_2H^+ fragment contained in these pairs is often observed with an appreciable intensity in mass spectra of methyl-containing organosilicon molecules, where SiC_2H^+ is produced from $CH_2SiCH_3^+$ by successive H_2 elimination. The $CH_2SiCH_3^+$ ion is produced from $CH_2Si(CH_3)_2^+$ by CH_3 elimination.[22] It can be expected that the $SiCH_2^+$ and $SiCH_3^+$ contained in the Si[F]-site-specific ion pairs are also produced from $CH_2Si(CH_3)_2^+$. Thus, it can be deduced that in the site-specific fragmentation caused by the Si[F]:2p ionization both of the $F-SiF_2-CH_2Si(CH_3)_3$ bonds around the initially core-ionized Si[F] site always dissociate.

The Si[Me]:2p ionization increases the production of $F_3SiCH_2Si(CH_3)_2^+-CH_3^+$, $SiF_3^+-CH_2Si(CH_3)_2^+$, and $F_2SiCH_2^+-Si(CH_3)_2F^+$ (Figure 5). The channel leading to the $F_2SiCH_2^+-Si(CH_3)_2F^+$ ion pair involves a migration of a F atom. The $F_3SiCH_2Si(CH_3)_2^+$, $CH_2Si(CH_3)_2^+$, and $Si(CH_3)_2F^+$ fragments in these three ion pairs are also the Si[Me]-site-specific ions, as can be seen from Figure 4. The production of all of these pairs requires the breaking of the Si[Me]−CH_3(methyl group) bond. This represents the characteristic of site-specific fragmentation caused by Si[Me]:2p ionization in FSMSM, although the corresponding characteristic in FSMSE is the Si[Me]−CH_2(bridge) bond dissociation, as mentioned above. Comparing the computed BDFs for Si[Me]:2p ionization, the BDF for the Si[Me]−CH_3(methyl group) bond is 0.02 higher in FSMSM than in FSMSE, whereas the BDF for the Si[Me]−CH_2(bridge) is 0.03 lower. While the difference is small, this is consistent with the experimental results. The results shown in Figure 5 also suggest that the Si[Me]:2p ionization of FSMSM may also increase the production of $CH_3^+-Si(CH_3)_2F^+$ and $SiF_3^+-Si(CH_3)H^+$ pairs. The main site-specific fragmentation patterns resulting from Si[F]:2p and Si[Me]:2p ionizations in FSMSM vapor were deduced from Figures 3−5 and are summarized in Figures S1 and S2 (Supporting Information). Site-specific bond dissociation occurs around the Si site where the photoionization has taken place. The calculated BDF values of FSMSM are given in Table S2.

As mentioned above, site-specific fragmentation is clearly revealed here. However, as shown in Figures 4 and 5, the branching ratios of the site-specific ions and ion pairs are not very large, and site-specific fragmentation tends to be obscured by other fragmentation processes. In the vapor phase, after the initial site-specific fragmentation step, the site specificity may be lost during second fragmentation steps, where some non-site-specific fragments may be produced. However, on a solid surface or in the bulk, reneatralization or recapture by the substrate or nearby atoms would protect the initially produced species from disintegration leading to smaller species through the above-mentioned second steps. Furthermore, Tinone et al.[16] expect that site-specific fragmentation should be easily observed on a solid surface because ions produced through fast energetic paths—such as site-specific fragmentation—are revealed selectively on a solid surface. This is also due to the efficient reneutralization or recapture of nonenergetic fragments. In contrast, all of the ions produced are collected by the ion detection apparatus in the vapor phase, and the resulting spectrum is a sum of all decomposition paths. It can be expected that a practical molecular knife would be used for surface or bulk molecules rather than for those in the vapor phase. As mentioned in the Introduction, the precise control of surface molecules is essential for the precision fabrication of electronic devices. Accordingly, controlled bond dissociation following photoionization of a localized core electron may be a candidate for a practical molecular knife[1,2] if we assume that the reneutralization and recapture suppress the desorption of slow ionic fragments

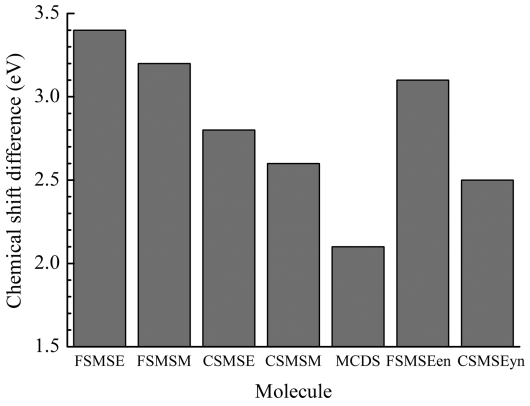

Figure 6. Difference between experimental Si[X]:2p and Si[Me]:2p binding energies (chemical shift difference) for HSMSB vapor. The individual binding energies and chemical shift differences are given in Table S1 (Supporting Information).

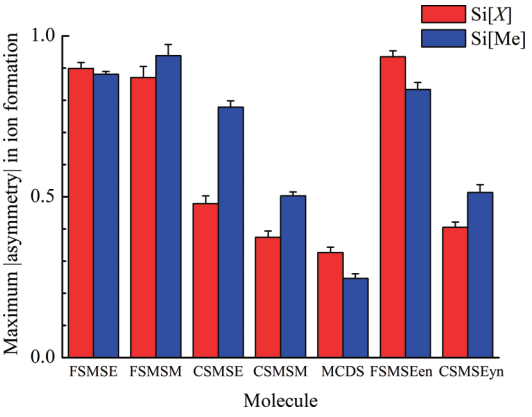

Figure 7. Maximum absolute value of asymmetry (maximum |asymmetry|) for ion formation by Si:2p ionization in HSMSB vapor. The red and blue bars show the values for Si[X]:2p and Si[Me]:2p ionizations, respectively. The asymmetry data are given in the EPAPS document of ref 20, Figure 4 of this paper, and Figures S4, S7, S10, S13, and S16 (Supporting Information).

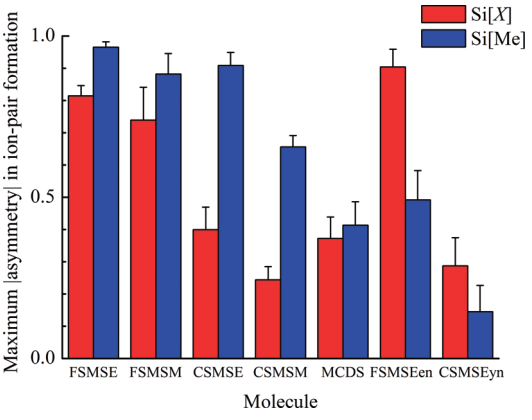

Figure 8. Maximum absolute value of asymmetry (maximum |asymmetry|) for ion-pair formation by Si:2p ionization in HSMSB vapor. The red and blue bars show the values for Si[X]:2p and Si[Me]:2p ionizations, respectively. The asymmetry data are given in the EPAPS document of ref 20, Figure 5 of this paper, and Figures S5, S8, S11, S14, and S17 (Supporting Information).

and protect the molecule from disintegration leading to atoms and/or small species.

4.4. CSMSE, CSMSM, MCDS, FSMSEen, and CSMSEyn. We have similarly studied the ionic fragmentation patterns and Si:2p chemical shifts of CSMSE, CSMSM, MCDS, FSMSEen, and CSMSEyn. In MCDS, CSMSM, and CSMSE ($Cl_3Si(CH_2)_n$-$Si(CH_3)_3$, $n = 0-2$), the Si[Cl] and Si[Me] sites are separated by increasing numbers of methylene units ($-CH_2-$). In MCDS, the Si[Cl] and Si[Me] sites are directly bonded to each other without any bridge between them. Especially, it is very important to examine how the direct intersite bonding in MCDS affects site specificity in fragmentation and the 2p chemical shift difference between the two sites because this may explain why the site specificity of acetone is not clearly revealed, as mentioned in the Introduction.

While the two Si sites are connected through a chain of three saturated bonds in FSMSE and CSMSE ($-CH_2-CH_2-$), the central saturated bond is replaced by an unsaturated bond in FSMSEen ($-CH{=}CH-$) and CSMSEyn ($-C{\equiv}C-$). In order to create a sharp molecular knife, we have examined how the replacement by the unsaturated bond affects site specificity.

In CSMSE and CSMSM, three Cl atoms are substituted for the three F atoms of FSMSE and FSMSM, respectively, but the bridges between the Si[Cl] and Si[Me] sites of CSMSE ($-CH_2CH_2-$) and CSMSM ($-CH_2-$) are the same as those of FSMSE and FSMSM. It is interesting how the substitution of Cl for F has an influence on the site specificity in fragmentation as well as on the chemical shift difference between Si[X]:2p and Si[Me]:2p.

The Si:2p PES, PEPICO spectra, and asymmetry and relative intensity of ion and ion-pair formation in CSMSE, CSMSM, MCDS, FSMSEen, and CSMSEyn vapors are given in Figures S3−S17 (Supporting Information). The Si[Me]:2p and Si[X]:2p binding energies and the difference between them are given in Table S1. The BDF values are given in Tables S3−S5. The ionic fragmentation processes caused by the Si:2p ionizations are also explained in detail in the Supporting Information. The main site-specific fragmentation patterns of CSMSE, CSMSM, and FSMSEen, which can be deduced from Figures S3−S8 and S12−S14, are summarized in Figures S18−S23. When site-specific bond dissociation appears in these molecules, it occurs around the Si site where the photoionization has taken place.

4.5. Comparison of Site Specificity among Different HSMSBs. Figure 6 shows the difference between the Si[X]:2p and Si[Me]:2p binding energies (chemical shift difference) in HSMSB vapor. A large chemical shift difference leads to clear site selection in the Si:2p PES. One may suppose that, if the peaks are clearly separated in the Si:2p PES, an increasing chemical shift difference does no longer increase the site specificity in fragmentation. We will show that this is not the case. Figures 7 and 8 show how the asymmetry defined in section 4.3 depends on the molecular structure of the HSMSB. As the absolute value of asymmetry (|asymmetry|) increases, site-specific fragmentation becomes evident. In Figure 7, the red bars show the absolute values of the maximum asymmetry (maximum |asymmetry|) in ion formation by Si[X]:2p ionization and the blue bars those for ion formation by Si[Me]:2p ionization. For example, in FSMSM, the red and blue bars respectively show the values of

Scheme 1. Schematic Representation of the Electron-Donating and -Accepting Properties of Methyl Groups and Cl Atoms at the Si[Me] and Si[Cl] Sites, Respectively[41]

MCDS

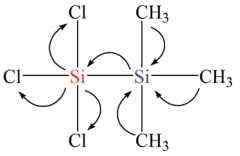

CSMSE

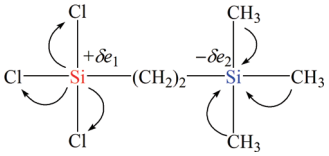

F^+ and $F_3SiCH_2Si(CH_3)_2^+$ (0.87 and 0.94) as shown in Figure 4. Similarly, Figure 8 shows the maximum |asymmetry| in ion-pair formation by Si:2p ionization in HSMSB vapor. Figures 6−8 are similar in appearance to one another. Thus, the chemical shift difference and the site specificity in fragmentation depend in a similar way on the intersite bridge and the electronegativity of the included halogen atoms. Even though the peaks in the Si:2p PES are clearly separated, the site specificity in fragmentation increases with increasing peak separation.

On the whole, the site specificity (chemical shift difference and asymmetry) of FSMSM is a little less than that of FSMSE. Furthermore, the specificity in CSMSE, CSMSM, and MCDS decreases as the bridge length between the two Si sites is reduced (Figures 6−8). Thus, the site specificity generally decreases as the bridge length decreases. A similar result was obtained for element-specific fragmentation of $CH_3CO(CH_2)_nCN$ (n = 0−3).[40] It can be expected that FSMSM would be roughly intermediate in site specificity between FSMSE and 1,1,1-trimethyltrifluorodisilane [$F_3SiSi(CH_3)_3$] if the latter molecule could be prepared (see section 2.1).

In MCDS, where the two Si sites are directly bonded to each other, the 2p chemical shift difference between the two sites greatly decreases (Figure 6 and Table S1), and also the asymmetry (site specificity in fragmentation) is nearly lost (Figures S9−S11), in contrast to CSMSE and CSMSM (Figures S3−S8) (also see Figures 7 and 8). The reduction of the site specificity in MCDS is probably due to efficient electron migration between the two Si sites (Scheme 1).[41] The electron-donating property (small electronegativity) of the $Si(CH_3)_3$ group and the electron-accepting property (large electronegativity) of the $SiCl_3$ group enhance the intersite electron migration from $Si(CH_3)_3$ to $SiCl_3$ in MCDS and cancel out the effects of the electron-donating property of the methyl groups and the electron-accepting property of the Cl atoms. As a result, the Si[Cl] and Si[Me] sites of MCDS cannot clearly be distinguished in view of electron distribution. However, the long intersite bridge of CSMSE maintains the site specificity by suppressing the intersite electron migration from $Si(CH_3)_3$ to $SiCl_3$ (Scheme 1).[41] CSMSM is roughly intermediate between CSMSE and MCDS. Since the C atoms in acetone are directly bonded to each other, as are the Si atoms in MCDS, intramolecular electron migration between the C sites can be expected to reduce site specificity in acetone in a similar way.

On the whole, the site specificity of FSMSEen is less than that of FSMSE (Figures 6−8). Furthermore, in CSMSEyn, the 2p chemical shift difference between the two Si sites greatly decreases (Figure 6 and Table S1), and also the asymmetry is nearly lost (Figures S15−S17), in contrast to CSMSE (Figures S3−S5). In FSMSEen and CSMSEyn where the central saturated bonds in the intersite bridges of FSMSE and CSMSE are replaced by double and triple bonds, respectively, the site specificity is generally reduced (Figures 6−8). The reduction of the site specificity can be explained by the enhancement of intramolecular electron migration between the two Si sites connected through an unsaturated bond. The increase in bond order generally strengthens the connection between the two C atoms in the intersite bridge and enhances the intersite electron migration. It is interesting that the decrease in maximum |asymmetry| on going from FSMSE to FSMSEen is greater in the Si[Me]:2p ionization (blue bar) than in the Si[F]:2p ionization (red bar) in Figures 7 and 8. This decrease derived from the experimental result is reproduced in the calculated BDF values (Tables S2 and S4). In FSMSEen, interaction similar to hyperconjugation[42] may be present between the methyl groups around Si[Me] and the central C═C bond in the intersite bridge.

The site specificities in CSMSE and CSMSM are less than those in FSMSE and FSMSM, respectively (Figures 6−8). Since the electronegativity of Cl is less than that of F, and closer to that of a methyl group bonded to Si[Me],[19] the substitution of Cl for F reduces the site specificity.

As shown in Figures 7 and 8, the decreases in maximum |asymmetry| on going from FSMSE and FSMSM to CSMSE and CSMSM are greater for Si[X]:2p ionization (red bars) than for Si[Me]:2p ionization (blue bars). By substituting Cl for F, the specificity for the Si[X] sites near the halogen atom X drops more than that for the Si[Me] sites, which are far away from the X atoms. At present, we cannot present an unambiguous reason for this result, but in a simple physical picture the following comments can be made. A decrease in electron-accepting nature around Si[X] due to the substitution may increase the valence-electron density at Si[X], which may approach that at Si[Me]. However, the substitution should not have a great influence on the valence-electron distribution at Si[Me] because the intersite bridge of these molecules suppresses efficient electron migration between Si[X] and Si[Me]. This explanation is consistent with the changes in Si:2p binding energy (Table S1) on going from FSMSE and FSMSM to CSMSE and CSMSM, respectively (see ref 8). As a result, the strongest effects are seen in the Si[X]-localized fragmentation processes caused by Si[X]:2p ionization, with the Si[Me]-localized processes remaining unchanged. This could explain the decrease in the Si[X] site specificity in fragmentation. However, further investigations are needed to clarify the reason for the greater decrease in the Si[X] site specificity due to substitution.

As described above, site-specific fragmentation in HSMSB molecules is enhanced when the intersite bridge is long, the bridge consists of saturated bonds, and X = F. The strongest site specificity among all the HSMSB molecules studied is found in FSMSE.

5. CONCLUSIONS

In an aim to create a "sharp" molecular knife, we have studied site-specific fragmentation caused by Si:2p core photoionization in HSMSB vapor. Highly site-specific bond dissociation has been

found to occur around the core-ionized Si site in some of the molecules studied. The site specificity in fragmentation and the 2p chemical shift difference between the two Si sites were found to depend in similar ways on the nature of the intersite bridge and on the electronegativity of the included halogen atoms. Even though the peaks in the Si:2p PES are clearly separated, the site specificity in fragmentation increases with increasing peak separation. The present experimental and computational results show that the following conditions should be satisfied for an effective molecular knife. First, the atomic sites to be distinguished between or "cut" should be located far from each other and connected through a chain of saturated bonds, so that intersite electron migration can be reduced. Second, the chemical environment of one atomic site should be as different as possible from that of the other atomic site, so that a resonant excitation of a core electron to an antibonding orbital can be used to selectively create a core hole at only one of the sites. Our results show a high site specificity for FSMSE because FSMSE has a long chain of saturated bonds between the two Si sites ($-CH_2CH_2-$), and the electronegativity difference between the F atom bonded to Si[F] and the methyl group bonded to Si[Me] is very large. It can be said that in FSMSE, $F_3Si-CH_2CH_2-Si(CH_3)_3$, there is no communication between the Si atoms at either end of the molecule. If we can select a particular atomic site among multiple atoms of the same element placed in various different chemical environments within a molecule and control core photoexcitaiton at this atomic site, site-specific fragmentation offers an approach to developing a "sharp" molecular knife. A detailed elucidation of the site-specific fragmentation mechanism may still require further work but will bring the goal of sub-nanoscale fabrication of various materials and other applications one step closer to realization.

■ ASSOCIATED CONTENT

Supporting Information. Si:2p PES, PEPICO spectra, asymmetry and relative intensity in ion and ion-pair formation, and detailed ionic fragmentation processes caused by Si:2p ionizations in CSMSE, CSMSM, MCDS, FSMSEen, and CSMSEyn vapors, Si:2p binding energies and BDF values of HSMSBs, main site-specific fragmentation patterns and mechanisms through which ions and ion pairs are produced by Si:2p ionization in FSMSM, CSMSE, CSMSM, and FSMSEen vapors, and complete ref 29. This material is available free of charge via the Internet at http://pubs.acs.org.

■ AUTHOR INFORMATION

Corresponding Author

*E-mail: nagaoka@ehime-u.ac.jp.

Present Addresses

[#]Hiroshima Synchrotron Radiation Center, Hiroshima University, Higashi-Hiroshima 739-0046, Japan.

[&]Japan Atomic Energy Agency/SPring-8, 1-1-1 Kouto, Sayo-cho, Sayo-gun 679-5198, Japan.

■ ACKNOWLEDGMENT

We express our sincere thanks to Professor Joji Ohshita of Hiroshima University for generously providing us with samples of the HSMSB molecules. We also thank Ms. Ayumi Shimizu and Mr. Shouta Arai of Ehime University, and also the SPring-8 facility staff for their kind help in the present study. S.N. is grateful to Dr. Umpei Nagashima of the Japanese National Institute of Advanced Industrial Science and Technology (AIST) for his help in Gaussian convolution and also valuable discussions. S.N. also thanks the Research Center for Computational Science at the Okazaki Research Facilities of the Japanese National Institutes of Natural Sciences for the use of their computers and the Library Program Gaussian 03. The experiments were carried out with the approval of JASRI (Proposal Nos. 2006A1176, 2006B1607, and 2007B1129) partly as a Nanotechnology Support Project of the Ministry of Education, Culture, Sports, Science, and Technology of Japan (MEXT).

■ REFERENCES

(1) Tanaka, K.; Kizaki, H.; Sumii, R.; Matsumoto, Y.; Wada, S. *Radiat. Phys. Chem.* **2006**, *75*, 2076–2079.

(2) Nagaoka, S.; Prümper, G.; Ueda, K. In *SPring-8 Research Frontiers 2008*; Kikuta, S., Ed.; SPring-8/JASRI: Sayo-cho, Sayo-gun, 2009; pp 114−115.

(3) Wagner, C. D.; Riggs, W. M.; Davis, L. E.; Moulder, J. F.; Muilenberg, G. E. *Handbook of X-ray Photoelectron Spectroscopy*; Perkin-Elmer: Eden Prairie, MN, 1979.

(4) Hitchcock, A. P.; Neville, J. J. In *Chemical Applications of Synchrotron Radiation, Part I: Dynamics and VUV Spectroscopy*; Sham, T.-K., Ed.; World Scientific: Singapore, 2002; Chapter 4.

(5) Nagaoka, S.; Takemoto, M.; Prümper, G.; Fukuzawa, H.; Tamenori, Y.; Suzuki, I. H.; Ueda, K. *J. Chem. Phys.* **2008**, *129*, 204309.

(6) Habenicht, W.; Baiter, H.; Müller-Dethlefs, K.; Schlag, E. W. *J. Phys. Chem.* **1991**, *95*, 6774–6780.

(7) Nagaoka, S.; Tanaka, S.; Mase, K. *J. Phys. Chem. B* **2001**, *105*, 1554–1561.

(8) Siegbahn, K.; Nordling, C.; Johansson, G.; Hedman, J.; Hedén, P. F.; Hamrin, K.; Gelius, U.; Bergmark, T.; Werme, L. O.; Manne, R.; Baer, Y. *ESCA Applied to Free Molecules*; North-Holland: Amsterdam, 1969; Section 5.4.

(9) Nagaoka, S. *J. Chem. Educ.* **2007**, *84*, 801–802.

(10) Eberhardt, W.; Sham, T. K.; Carr, R.; Krummacher, S.; Strongin, M.; Weng, S. L.; Wesner, D. *Phys. Rev. Lett.* **1983**, *50*, 1038–1041.

(11) Suzuki, I. H.; Saito, N. *Chem. Phys.* **2000**, *253*, 351–359.

(12) Suzuki, I. H.; Saito, N. *Int. J. Mass Spectrom.* **2000**, *198*, 165–172.

(13) Romberg, R.; Heckmair, N.; Frigo, S. P.; Ogurtsov, A.; Menzel, D.; Feulner, P. *Phys. Rev. Lett.* **2000**, *84*, 374–377.

(14) Nagaoka, S.; Mase, K.; Nakamura, A.; Nagao, M.; Yoshinobu, J.; Tanaka, S. *J. Chem. Phys.* **2002**, *117*, 3961–3971.

(15) Mase, K.; Kobayashi, E.; Nambu, A.; Kakiuchi, T.; Takahashi, O.; Tabayashi, K.; Ohshita, J.; Hashimoto, S.; Tanaka, M.; Nagaoka, S. *Surf. Sci.*, to be submitted.

(16) Tinone, M. C. K.; Tanaka, K.; Maruyama, J.; Ueno, N.; Imamura, M.; Matsubayashi, N. *J. Chem. Phys.* **1994**, *100*, 5988–5995.

(17) Muller, D. A.; Sorsch, T.; Moccio, S.; Baumann, F. H.; Evans-Lutterodt, K.; Timp, G. *Nature* **1999**, *399*, 758–761.

(18) International Technology Roadmap for Semiconductors Home Page. http://www.itrs.net/ (accessed July 2011).

(19) Carlson, T. A. *Photoelectron and Auger Spectroscopy*; Plenum: New York, 1975; Section 5.2.

(20) Nagaoka, S.; Prümper, G.; Fukuzawa, H.; Hino, M.; Takemoto, M.; Tamenori, Y.; Harries, J.; Suzuki, I. H.; Takahashi, O.; Okada, K.; Tabayashi, K.; Liu, X-J.; Lischke, T.; Ueda, K. *Phys. Rev. A* **2007**, *75*, 020502(R) (4 pages).

(21) Nagaoka, S.; Ohshita, J.; Ishikawa, M.; Masuoka, T.; Koyano, I. *J. Phys. Chem.* **1993**, *97*, 1488–1495.

(22) Nagaoka, S.; Ohshita, J.; Ishikawa, M.; Takano, K.; Nagashima, U.; Takeuchi, T.; Koyano, I. *J. Chem. Phys.* **1995**, *102*, 6078–6087.

(23) Nagaoka, S.; Fujibuchi, T.; Ohshita, J.; Ishikawa, M.; Koyano, I. *Int. J. Mass Spectrom. Ion Processes* **1997**, *171*, 95–103.
(24) Nagaoka, S.; Fujibuchi, T.; Ohshita, J.; Nagashima, U.; Koyano, I. *Chem. Phys.* **2002**, *276*, 243–256.
(25) Prümper, G.; Tamenori, Y.; De Fanis, A.; Hergenhahn, U.; Kitajima, M.; Hoshino, M.; Tanaka, H.; Ueda, K. *J. Phys. B* **2005**, *38*, 1–10.
(26) Prümper, G.; Fukuzawa, H.; Lischke, T.; Ueda, K. *Rev. Sci. Instrum.* **2007**, *78*, 083104.
(27) Ohashi, H.; Ishiguro, E.; Tamenori, Y.; Kishimoto, H.; Tanaka, M.; Irie, M.; Tanaka, T.; Ishikawa, T. *Nucl. Instrum. Methods Phys. Res., Sect. A* **2001**, *467−468*, 529–532.
(28) Sugar, J.; Musgrove, A. *J. Phys. Chem. Ref. Data* **1991**, *20*, 859–915.
(29) Frisch, M. J. et al. *Gaussian 03, Revision C.02*; Gaussian, Inc.: Wallingford, CT, 2004.
(30) Takahashi, O.; Mitani, M.; Joyabu, M.; Saito, K.; Iwata, S. *J. Electron Spectrosc. Relat. Phenom.* **2001**, *120*, 137–148.
(31) Mitani, M.; Takahashi, O.; Saito, K.; Iwata, S. *J. Electron Spectrosc. Relat. Phenom.* **2003**, *128*, 103–117.
(32) Siegbahn, H.; Asplund, L.; Kelfve, P. *Chem. Phys. Lett.* **1975**, *35*, 330–335.
(33) Carroll, T. X.; Thomas, T. D. *J. Chem. Phys.* **1990**, *92*, 7171–7177.
(34) Nagaoka, S.; Nitta, A.; Tamenori, Y.; Fukuzawa, H.; Ueda, K.; Takahashi, O.; Kakiuchi, T.; Kitajima, Y.; Mase, K.; Suzuki, I. H. *J. Electron Spectrosc. Relat. Phenom.* **2009**, *175*, 14–20.
(35) Imamura, T.; Brion, C. E.; Koyano, I.; lbuki, T.; Masuoka, T. *J. Chem. Phys.* **1991**, *94*, 4936–4948.
(36) Boo, B. H.; Park, S. M.; Koyano, I. *J. Phys. Chem.* **1995**, *99*, 13362–13367.
(37) Santos, A. C. F.; Lucas, C. A.; de Souza, G. G. B. *Chem. Phys.* **2002**, *282*, 315–326.
(38) Suzuki, I. H.; Nitta, A.; Shimizu, A.; Tamenori, Y.; Fukuzawa, H.; Ueda, K.; Nagaoka, S. *J. Electron Spectrosc. Relat. Phenom.* **2009**, *173*, 18–23.
(39) Prümper, G.; Liu, X. J.; Fukuzawa, H.; Ueda, K.; Carravetta, V.; Harries, J.; Tamenori, Y.; Nagaoka, S. *J. Phys.: Conf. Ser.* **2007**, *88*, 012008.
(40) Okada, K.; Tanimoto, S.; Morita, T.; Saito, K.; Ibuki, T.; Gejo, T. *J. Phys. Chem. A* **2003**, *107*, 8444–8448.
(41) Nagaoka, S.; Nagashima, U.; Ohshita, J. *Bull. Chem. Soc. Jpn.* **2006**, *79*, 537–548.
(42) Vollhardt, K. P. C.; Schore, N. E. *Organic Chemistry Structure and Function*, 6th ed.; Freeman: New York, 2011; Section 3.2.